Agricultural and Forest Meteorology 301–302 (2021) 108343

Contents lists available at ScienceDirect

Agricultural and Forest Meteorology

journal homepage: www.elsevier.com/locate/agrformet

Connotation analysis of parameters in the generalized nonlinear advection aridity model

Haixiang Zhou[a,c], Zhi Li[b], Wenzhao Liu[a,c,*]

[a] State Key Laboratory of Soil Erosion and Dryland Farming on the Loess Plateau, Institute of Soil and Water Conservation, Northwest A&F University, Yangling, 712100, China
[b] College of Natural Resources and Environment, Northwest A&F University, Yangling, 712100, China
[c] University of Chinese Academy of Sciences, Beijing 100049, China

ARTICLE INFO

Keywords:
Evaporation
Generalized complementary evaporation relationship
GNAA
Priestley-Taylor parameter
Loess plateau

ABSTRACT

The generalized nonlinear advection aridity model (GNAA) for evaporation (E) estimation can be expressed in a basic form with a single parameter $\alpha_{e\text{-}0}$, or an extended form using two parameters, $\alpha_{e\text{-}c}$ and c. The implications of these model parameters in the model and the accurate estimation of E are receiving increasing attention. Our study shows that $\alpha_{e\text{-}0}$ and $\alpha_{e\text{-}c}$ are affected by precipitation (P), the aridity index (E_{pa}/P) and the climate seasonality and asynchrony index (*SAI*), etc, with which $\alpha_{e\text{-}0}$ has stronger correlations. This demonstrated that annual $\alpha_{e\text{-}0}$ and $\alpha_{e\text{-}c}$ could cover the α parameter in the Priestley–Taylor formula, as well as other factors, particularly the aridity index. For the basic GNAA form, annual $\alpha_{e\text{-}0}$ is smaller than 1.00 in most catchments, but the GNAA model with the developed empirical formula between $\alpha_{e\text{-}0}$ and E_{pa}/P can accurately estimate E at an annual scale. For the extended GNAA form, most annual $\alpha_{e\text{-}c}$ were larger than 1.00, with a mean value of 1.08 for the Loess Plateau; $\alpha_{e\text{-}c}$ tended to restore the original α values in the Priestley-Taylor equation. Functional differences exist between the basic and extended GNAA forms in estimating E and explaining the complementary relationship. Our results bridge some gaps in understanding the GNAA model from previous studies, and provide useful information to extend the application of the GNAA model.

1. Introduction

The evaporation (E), which is equivalent to the term "evapotranspiration" in this study, plays a unique role in linking the terrestrial water cycle and energy balance (Brutsaert, 1982). However, the complexity associated with the soil–plant–atmosphere continuum hinders the accurate estimation or measurement of E, causing errors of up to 50% in the global annual average E estimated with different models and datasets (Jimenez et al., 2011). Under such a background, previous studies have made significant efforts to improve the accuracy of E estimates. The complementary relationship (CR) between E and the apparent potential evaporation, E_{pa}, provides an important theoretical framework for E estimation. CR interprets the mechanism of vapor transport and its feedback in the land–atmosphere system, effectively estimating E via conventional meteorological data without the need for soil and vegetation information. However, issues related to the application and theoretical background of CR require further investigation.

Bouchet (1963) first proposed the conceptual CR model with a single boundary condition under a completely wetting condition. The algorithms for variable estimation, however, were not clear. Subsequently, several models have been proposed for E estimation using the CR framework, including the AA (Brutsaert and Stricker, 1979), the CRAE (Morton, 1978, 1983), and the Granger (Granger, 1989) models. Referring to the Budyko hypothesis (Budyko, 1974; Budyko, 1948), three additional boundaries to the CR under extreme climate conditions were introduced, and several generalized complementary functions were proposed (Brutsaert, 2015; Gao and Xu, 2020; Han et al, 2012; Han and Tian, 2018), which promotes CR with stricter boundaries toward a generalized direction via nonlinear functions (Han and Tian, 2020). Brutsaert (2015) modified the boundaries proposed by Han et al. (2012) and redefined the concepts of two potential evaporations to propose a polynomial formulation, i.e., the generalized nonlinear advection aridity (GNAA) model. In the GNAA model, E_{po} is the potential evaporation that occurs at a saturated, sufficiently large and homogeneous surface while E_{pa} is the apparent potential evaporation that occurs at a small wet patch inside the large non-wet surface.

There are two forms of GNAA model, where the basic form in

* Corresponding author.
E-mail address: wzliu@ms.iswc.ac.cn (W. Liu).

https://doi.org/10.1016/j.agrformet.2021.108343
Received 28 July 2020; Received in revised form 12 January 2021; Accepted 21 January 2021
Available online 26 February 2021

Notation

α	the Priestley–Taylor parameter, dimensionless
$\alpha_{e\text{-}0}$	analog of the Priestley–Taylor parameter in the basic GNAA (an adjustable parameter), dimensionless
$\alpha_{e\text{-}c}$	analog of the Priestley–Taylor parameter in the extended GNAA (an adjustable parameter), dimensionless
c	an adjustable parameter in the extended GNAA, dimensionless
E	evaporation, or actual evaporation, mm/year
E_e	equilibrium evaporation or radiation term in the Penman equation, mm/day or mm/year
E_{GLEAM}	evaporation from the GLEAM product, mm/year
E_{po}	potential evaporation, mm/day or mm/year
E_{pa}	apparent potential evaporation, mm/day or mm/year
E_{wb}	E calculated by the water balance method, mm/year
P	mean annual precipitation, mm/year
R	mean annual runoff, mm/year
ΔS	water storage variation, mm/year
SAI	climate seasonality and asynchrony index, dimensionless
x	independent variable, $x = E_e/E_{pa}$, dimensionless
x_B	independent variable defined by Brutsaert (2015), $x_B = E_{po}/E_{pa}$, dimensionless
$x_{B,min}$	minimum value of x_B at y=0 in GNAA, dimensionless
y	scaled evaporation, $y = E/E_{pa}$, dimensionless

dimensionless is as follows:

$$y = 2{x_B}^2 - {x_B}^3 \quad (1)$$

where $y = E/E_{pa}$ and $x_B = E_{po}/E_{pa}$. Brutsaert (2015) recommended Eq. (1) for E estimation, but also presented a quartic polynomial equation with a tuneable parameter c as an extended form to accommodate some datasets,

$$y = (2-c){x_B}^2 - (1-2c){x_B}^3 - c{x_B}^4 \quad (2)$$

Eq. (2) becomes (1) when c is equal to 0. For each GNAA form, E_{pa} and E_{po} can be estimated by the Penman equation (Penman, 1948) and Priestley–Taylor (hereinafter denoted as P-T) equation (Priestley and Taylor, 1972), respectively.

$$E_{pa} = \frac{\Delta}{\Delta+\gamma}(R_n - G) + \frac{\gamma}{\Delta+\gamma} f(u_2)\left(e_a^* - e_a\right) \quad (3)$$

$$E_{po} = \alpha\frac{\Delta}{\Delta+\gamma}(R_n - G) = \alpha E_e \quad (4)$$

where $\Delta = \frac{d(e_a^*)}{d(T_a)}$ is the slope of the saturation vapor pressure versus T_a (hPa/°C); γ is the psychrometric constant (hPa/°C); R_n is the net radiation (mm/day), calculated using the sunshine duration, latitude, and other factors (Allen et al., 1998) ; G is the surface heat flux (mm/day), being zero on a daily scale in this study; e_a* is the saturation vapor pressure at the actual air temperature (hPa); e_a is the actual vapor pressure (hPa); $f(u_2)$ is the wind function at a height of 2 m [i.e., $f(u_2) = 0.26(1 + 0.54u_2)$, where $u_2 = u_{10}\,(2/10)^{1/7}$]; and E_e in the right term of Eq. (4) is the equilibrium evaporation (Slatyer and Mcilroy, 1961). There exists a parameter in the P-T equation, i.e., α. When Eq. (4) is used in the GNAA, α is replaced by $\alpha_{e\text{-}0}$ and $\alpha_{e\text{-}c}$ in the basic and extended GNAA forms, respectively. $\alpha_{e\text{-}0}$ and $\alpha_{e\text{-}c}$represent the adjustable parameters, analogs of the P-T coefficient (Brutsaert et al., 2017, 2020).

Using x to represent E_e/E_{pa}, the extended form of GNAA can be rewritten as follows:

$$y = (2-c)(\alpha_{e-c}x)^2 - (1-2c)(\alpha_{e-c}x)^3 - c(\alpha_{e-c}x)^4 \quad (5)$$

When using the GNAA model for E estimation, we must calibrate the parameters of $\alpha_{e\text{-}0}$, $\alpha_{e\text{-}c}$ and c in the basic or extended GNAA forms. Previous studies have shown that the values of $\alpha_{e\text{-}0}$ and $\alpha_{e\text{-}c}$ vary with time scales, regions, etc. Specifically, the parameter $\alpha_{e\text{-}0}$ at a daily scale was found to range from 1.04 to 1.19 for four land cover types in Australia (Zhang et al., 2017), 1.01 to 1.02 at three heights with different flux sources throughout the southern Loess Plateau (Brutsaert et al., 2017), 0.98 to 1.13 for four sites with four vegetation types along an elevation gradient of Mount Gongga in southwest China (Hu et al., 2018), and 0.95 to 1.05 for four sites in Japan (Ai et al., 2017). At the multi-year scale, $\alpha_{e\text{-}0}$ was found to range from 0.84 to 1.44 based on 241 catchments with different climate conditions in the eastern monsoon region of China ((X. Liu et al., 2016), and had a value of 0.705 in the Tarim River Basin of northwest China (Yu et al., 2019). Brutsaert et al. (2020) examined global surface evaporation using the basic GNAA form, indicating a wider range of $\alpha_{e\text{-}0}$ values. Han and Tian (2018) used the data from 20 flux stations to calibrate $\alpha_{e\text{-}c}$ and presented values ranging between 0.9 and 1.29 for the extended GNAA form. Furthermore, a previous study reported an $\alpha_{e\text{-}c}$ value of 1.09 for the United States at continental-scale, and suggested that the range of the parameter c should be limited to [–1, 2] to ensure that y increases monotonically with x and $y \le x$ for $0 \le x \le 1$ (Szilagyi et al., 2016). Liu et al. (2020), however, proposed the upper limit of c to be greater than 2. Zhou et al. (2020) found that there should be an adjustment of the parameters $\alpha_{e\text{-}c}$ and c to the GNAA curve, demonstrating that it is necessary to calibrate both $\alpha_{e\text{-}c}$ and c when estimating annual E. X. Liu et al. (2018), however, believed that E was not sensitive to c at a daily scale, and the basic GNAA form could accurately estimate E. Brutsaert et al. (2020) estimated global E values at multi-year scale by means of the basic GNAA form. In the light of these inconsistent results, it remains unclear which form is more effective in estimating E.

Moreover, it is a problem how to get rational $\alpha_{e\text{-}0}$ and/or $\alpha_{e\text{-}c}$, and c parameters. Some studies first calibrated the parameter $\alpha_{e\text{-}0}$ based on known values of E (Hu et al., 2018; X. Liu et al., 2016; Yu et al., 2019), then estimated E with longer time series using the basic GNAA model. Other studies tried to build a function to calculate the parameter by other factors. X. Liu et al. (2016) explored the effects of climatic factors, soil moisture, vegetation conditions, E_{pa}, and the aridity index (E_{pa}/P) on $\alpha_{e\text{-}0}$, found that E_{pa}/P is the most important factor at a multi-year scale, and then developed an empirical function between $\alpha_{e\text{-}0}$ and E_{pa}/P. Brutsaert et al. (2020) established a semi-empirical function based on the relationship between $\alpha_{e\text{-}0}$ and E_{pa}/P, and Li et al. (2021) constructed a function of $\alpha_{e\text{-}0}$ with both E_{pa}/P and the Normalized Difference Vegetation Index during the growing season on the Loess Plateau. Hu et al. (2018), however, reported that $\alpha_{e\text{-}0}$ is related to the vegetation structure and is independent of the climate conditions at various elevations on Mount Gongga at the daily scale. Therefore, the factors controlling $\alpha_{e\text{-}0}$ appear to vary with conditions (X. Liu et al., 2016; Yang et al., 2013), which requires further investigation.

Based on these problems associated with GNAA, the objectives of this study were to 1) identify the factors controlling the $\alpha_{e\text{-}0}$ and $\alpha_{e\text{-}c}$ parameters, 2) investigate the applicability of basic GNAA form in estimating E at the annual scale, and 3) explore the implication of parameters in GNAA. This study provides insights into the conflicting interpretations of previous studies and extends the potential application of the GNAA method.

2. Materials and methods

2.1. Study region and data

We selected 10 catchments from the Loess Plateau of China to test the GNAA. The Loess Plateau is located in the upper and middle reaches of the Yellow River. It has an area of 6.4×10^5 km^2 with arid, semiarid, and sub-humid climates. Frequent rainstorms, erodible loess, steep slopes, and sparse vegetation coverage all result in the most severe soil erosion in the world (Fu et al., 2000; Tang, 1998).

Daily climate data were collected from 123 weather stations maintained by the China Meteorological Administration (http://data.cma.cn/) for the period of 1960 – 2012; the data include mean daily temperature (T_a), wind speed (u_{10}) at a height of 10 m above the surface, mean relative humidity (*RH*), sunshine duration (*SD*), and precipitation (*P*). Runoff data were collected from the Loess Plateau Data Centre (http://loess.geodata.cn). The daily values of E_{pa}, E_e, and P at each site were summed to obtain monthly values, which were then spatially averaged with the ordinary Kriging interpolation algorithm (Delhomme, 1987). We noted that different interpolation methods had little influence on the spatial average of E_{pa}, E_e, and P, as well as on the parameters (Zhou et al., 2020). The 10 catchments had areas ranging from 3,175 to 43,216 km^2, and their hydrometeorological characteristics and locations are respectively presented in Table S1 and Fig. 1.

The land surface has changed significantly because of soil conservation measures, including the construction of terraces and sediment-trapping dams since the 1950s (Zhang et al., 2008), and the initiation of large-scale revegetation projects since 1999 (Feng et al., 2016). Owing to the effects of soil conservation measures, the hydrological cycle has been significantly perturbed over time. All of the observed *E* data (i.e., E_{wb} in Section 2.2) from 1960 to 2011 were thus used to calibrate the parameters in GNAA. Furthermore, some typical long-term *E* products with high spatial resolutions, such as the Global Land Evaporation Amsterdam Model (GLEAM; https://www.gleam.eu/#home; Martens et al., 2017), Penman-Monteith-Leuning (PML) model (https://data.csiro.au/dap/landingpage?pid=csiro:17375&v=2&d=true; Zhang et al., 2016), GLDAS_Noah (https://disc.gsfc.nasa.gov/datasets/GLDAS_NOAH025_M_2.1/summary?keywords=GLDAS; Chen and Dudhia, 2001), and FLUXNET- model tree ensembles (FLUXNET-MTE; https://www.bgc-jena.mpg.de/geodb/projects/Home.php; Jung et al., 2011), were considered to validate the *E* values derived from GNAA model. Previous studies have shown that the GLEAM evaporation product performed well at estimating the annual *E* in China (W. Liu et al., 2016; Yang et al., 2018; Zhang et al., 2020), especially in dry regions (Ma et al., 2019). We further compared the performances of these products and found that the GLEAM data perform better in representing the observed *E* (Table S2). Therefore, the GLEAM evaporation product was used to validate the simulated *E* from 1980 to 2011.

2.2. Annual water balance equation and observed E data

The actual evaporation was derived using the water balance method at the catchment scale as follows:

$$E_{wb} = P - R - \Delta S \tag{6}$$

where E_{wb}, P, R, and ΔS are the annual actual evaporation, precipitation, runoff, and change in water storage, respectively. Most studies based on GRACE data have found that water storage has no clear variation (Zhao et al., 2011) or does not change significantly after 2007 (1.3mm/year; Mo et al., 2016), and that ΔS shows an insignificant negative trend in the Yellow River basin (less than 0.1 mm/month ; Lv et al., 2019) and could be negligible in the upper Yellow River basin (Xue et al., 2013). It is thus reasonable to assume ΔS to be zero. To further minimize the impacts of ΔS on the annual water balance, each variable in Eq. (6) was estimated for the hydrological year instead of the calendar year (Carmona et al., 2014; Sivapalan et al., 2011). In general, a hydrological year is defined as a period from the beginning of the rainy season to the end of the dry season of the following year. On the Loess Plateau, as more than 60% of annual precipitation occurs from June to October, but significantly increases from May, the hydrological year was defined as May to April of the following year.

2.3. GNAA parameter estimation and model evaluation

The parameter $\alpha_{e\text{-}0}$ was determined for each hydrological year by minimizing the absolute difference (AD) between the GNAA-simulated E_{mol} and observed E_{wb}.

$$\mathrm{AD} = \left| E_{mol,i} - E_{wb,i} \right| \tag{7}$$

where i denotes the time series. We set the range of $\alpha_{e\text{-}0}$ to 0.3–1.5 and

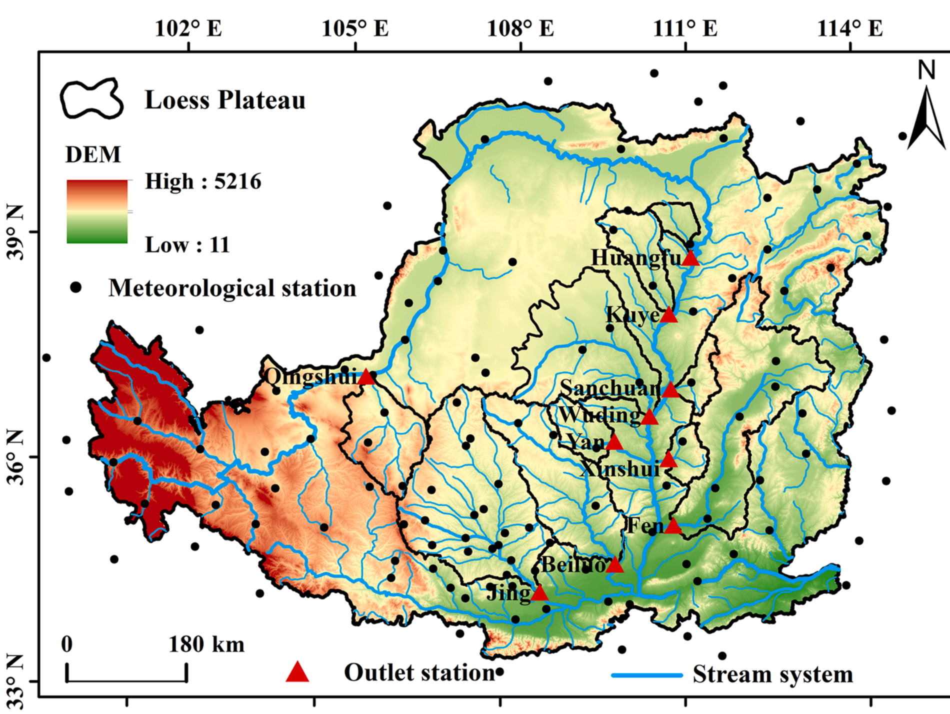

Fig. 1. Locations of the 10 catchments and meteorological stations in the Loess Plateau.

then continuously calculated AD with an interval of 0.001. The best model parameter was determined as the one with the smallest AD.

For the extended GNAA form, the parameter c need to be fixed when $\alpha_{e\text{-}c}$ is being calibrated using Eq. (7). The parameters $\alpha_{e\text{-}c}$ and c were first obtained by minimizing the mean absolute error (MAE; Eq. (8)) between E_{mol} and E_{wb} for each catchment, and then the annual value of $\alpha_{e\text{-}c}$ was obtained with Eq. (7) by setting c as its long-term mean value.

$$MAE = \frac{\sum_{i=1}^{n} \left| E_{mol,i} - E_{wb,i} \right|}{n} \tag{8}$$

where n denotes the length of the time sequence.

The values of estimated E were evaluated with the MAE, root mean square error (RMSE), and Nash-Sutcliffe efficiency coefficient (NSE).

3. Results

3.1. Calibrated parameters $\alpha_{e\text{-}0}$ and $\alpha_{e\text{-}c}$

At the annual scale, the parameter $\alpha_{e\text{-}0}$ in the basic GNAA form ranged from 0.39 to 1.05 in the 10 catchments, with a mean and standard deviation of 0.76 and 0.104, respectively. The mean annual $\alpha_{e\text{-}0}$ ranged from 0.68 to 0.83 in 10 catchments (Table 1). Spatially, the mean annual $\alpha_{e\text{-}0}$ values were greater in the south than those in the north. X. Liu et al. (2016) recognized that inaccurate precipitation observations from the Chinese Standard Precipitation Gauge (CSPG) owing to wetting loss and wind-induced undercatch (Goodison et al., 1989; Sevruk and Hamon,1984; Yang et al., 1999; X. Liu et al., 2016) may result in the errors for parameter calibration. We thus corrected the precipitation (P_c) according to X. Liu et al. (2016), and found that P_c was higher than P by 12%–18% (Table S1). If E was estimated with the corrected precipitation, the annual $\alpha_{e\text{-}0}$ ranged from 0.46 to 1.14 with a mean annual value of 0.75–0.91 (Table 1). The parameter α_e calculated by $P_c - R$ was 1.09 times of that calculated by $P - R$, but was still smaller than 1.0, implying the correction of precipitation had little impacts on the values of $\alpha_{e\text{-}0}$. In addition, most studies have used P data from CSPG as the ground-based truthful data. For the extended GNAA form, the optimized $\alpha_{e\text{-}c}$ and c parameters ranged from 0.91 to 1.18 and 2.73 to 11.18, with arithmetic mean values of 1.08 and 6.76, respectively (Table 1). When the c parameter was fixed as 6.76 for the Loess Plateau, the annual $\alpha_{e\text{-}c}$ estimated by Eq. (7) ranged from 1.0 to 1.22, with mean annual values of 1.08–1.11 for each catchment, and with no obvious spatial variation trend.

3.2. Controlling factors of $\alpha_{e\text{-}0}$ and $\alpha_{e\text{-}c}$

Besides the independent variables in Eq. (5) and Eq. (6), the effects of the aridity index (E_{pa}/P) were considered, referring to X. Liu et al. (2016). In particular, the seasonal distribution and matching condition between the potential evaporation and precipitation within a year were taken into account as they have a significant impact on E (J. Liu et al., 2018; Milly, 1994; Woods, 2003), which is represented by the climate seasonality and asynchrony index (SAI). The seasonal variations of P and E_{pa} can be described by sinusoidal functions. Milly (1994) and Woods (2003) proposed seasonality index only considering the 'mismatch' between seasonal amplitudes of P and E_{pa}. Berghuijs and Woods (2016) presented the asynchrony of P and air temperature, and J. Liu et al. (2018) improved SAI by incorporating the asynchrony of P and E_{pa}. Ning et al. (2019; 2020) further found that SAI with a fixed phase determined by the mean monthly P and E_{pa} performed better than the former (see details in the Supplementary Materials).

For the basic GNAA form, P, E_{pa}/P, and SAI all had significant effects on $\alpha_{e\text{-}0}$. A linear relationship existed between P and $\alpha_{e\text{-}0}$ with R^2 of 0.94. For the relationship between $\alpha_{e\text{-}0}$ and E_{pa}/P, Brutsaert et al. (2020) proposed the formula $\alpha_{e\text{-}0} = a/[1 + (b*E_{pa}/P)^c]$. We estimated the three coefficients (i.e., a, b, and c) with 'a' limited to [1.0, 1.5] because $\alpha_{e\text{-}0}$ has the range of [1.0, 1.5] under very wet condition (Brutsaert et al., 2020; Chen and Brutsaert, 1995). Fig. 2(d) shows the coefficients of a = 1.5, b = 0.38, and c = 0.92, as well as the function, with R^2 of 0.93, for the Loess Plateau. Similarly, SAI reflected the matching characteristics of P and E_{pa}, and indicated the asynchrony of water and energy distribution. The zero value of SAI means the best match between P and E_{pa} in the amplitude and time-phase during seasonal change. Thus, a function form similar to that given by Brutsaert et al. (2020) was used to fit the relationship between $\alpha_{e\text{-}0}$ and SAI, with R^2 of 0.87 (Fig. 2g). In general, P and E_{pa}/P reflect the surface moisture status. E_{pa}/P integrates the input and output demands of water, which are dimensionless and more comprehensive than P. Although SAI had a significant effect on the $\alpha_{e\text{-}0}$ parameter, it exhibits a significant linear relationship with E_{pa}/P (R^2 = 0.94), suggesting a collinearity problem. Accordingly, we considered the function between $\alpha_{e\text{-}0}$ and E_{pa}/P to be as follows:

$$\alpha_{e-0} = 1.5 \Big/ \left[1 + \left(0.38 E_{pa}/P \right)^{0.92} \right] \tag{9}$$

For the extended GNAA form, the influencing factors of $\alpha_{e\text{-}c}$ were similar to those of $\alpha_{e\text{-}0}$; we conducted the same analysis for the factors controlling annual $\alpha_{e\text{-}c}$ with a fixed c of 6.76. A linear relationship existed between $\alpha_{e\text{-}c}$ and P (R^2 = 0.39), whereas the functions proposed by Brutsaert et al. (2020) were used to describe the relationship between $\alpha_{e\text{-}c}$ and E_{pa}/P and SAI, with R^2 values of 0.29 and 0.26, respectively (Fig. 3). All the R^2 values between $\alpha_{e\text{-}c}$ and these factors were smaller than those between $\alpha_{e\text{-}0}$ and the factors. The relationship between $\alpha_{e\text{-}c}$ and E_{pa}/P was used to construct the function of $\alpha_{e\text{-}c}$ as:

$$\alpha_{e-c} = 1.5 \Big/ \left[1 + \left(0.0058 E_{pa}/P \right)^{0.24} \right] \tag{10}$$

Table 1
Values of $\alpha_{e\text{-}0}$ and $\alpha_{e\text{-}c}$ based on different approaches for the 10 catchments.

		Basic GNAA form		Extended GNAA form		
ID	Name	$\alpha^{a}_{e\text{-}0}$	$\alpha^{b}_{e\text{-}0}$	$\alpha^{d}_{e\text{-}c}$	c	$\alpha^{e}_{e\text{-}c}$
C1	Beiluo	0.83	0.92	1.09	6.45	1.10
C2	Fen	0.80	0.86	1.08	5.89	1.10
C3	Huangfu	0.71	0.78	0.91	2.73	1.09
C4	Jing	0.80	0.88	1.10	7.99	1.08
C5	Kuye	0.68	0.75	1.06	5.66	1.10
C6	Qingshui	0.69	0.76	1.04	5.70	1.08
C7	Sanchuan	0.76	0.82	1.18	11.18	1.09
C8	Wuding	0.71	0.79	1.11	6.91	1.11
C9	Xinshui	0.81	0.88	1.13	7.51	1.11
C10	Yan	0.79	0.88	1.09	7.61	1.08
Mean		0.76	0.83	1.08	6.76	1.09

Note: Superscripts a and b respectively correspond to P (precipitation) and P_c (corrected precipitation) when calculating E_{wb} during $\alpha_{e\text{-}0}$ calibration for a catchment. The $\alpha^{d}_{e\text{-}c}$ was obtained using Eq. (8), and $\alpha^{e}_{e\text{-}c}$ and c were obtained by using Eq. (7) with c fixed as 6.76.

3.3. Comparison of E estimation with different parameterisation schemes by GNAA

The performance of GNAA in E estimation was evaluated by comparing the interannual variation and annual values of estimated E with the GLEAM evaporation product (E_{GLEAM}). Note that values of E_{wb} were 1.1-fold of E_{GLEAM} for the Loess Plateau, and the correlation coefficient (r), MAE and NSE between E_{wb} and E_{GLEAM} were 0.83, 53.1mm/year, and 0.47, respectively (Fig. S1). When the GNAA model was applied to estimate E, the $\alpha_{e\text{-}0}$ and $\alpha_{e\text{-}c}$ parameters were obtained based on four schemes: 1) adopting $\alpha_{e\text{-}0}$ ($c = 0$) in the basic GNAA form for each catchment listed in Table 1; 2) adopting $\alpha_{e\text{-}c}$ ($c = 6.76$) in the extended GNAA form for each catchment listed in Table 1; 3) calculating $\alpha_{e\text{-}0}$ ($c = 0$) in the basic GNAA form with Eq. (9), and (4) calculating $\alpha_{e\text{-}c}$ ($c = 6.76$) in the extended GNAA form with Eq. (10). The simulated E, based on these four parameterization schemes were denoted briefly as E_0, E_c, E_{0f}, and E_{cf}, respectively. Compared with the interannual variation in

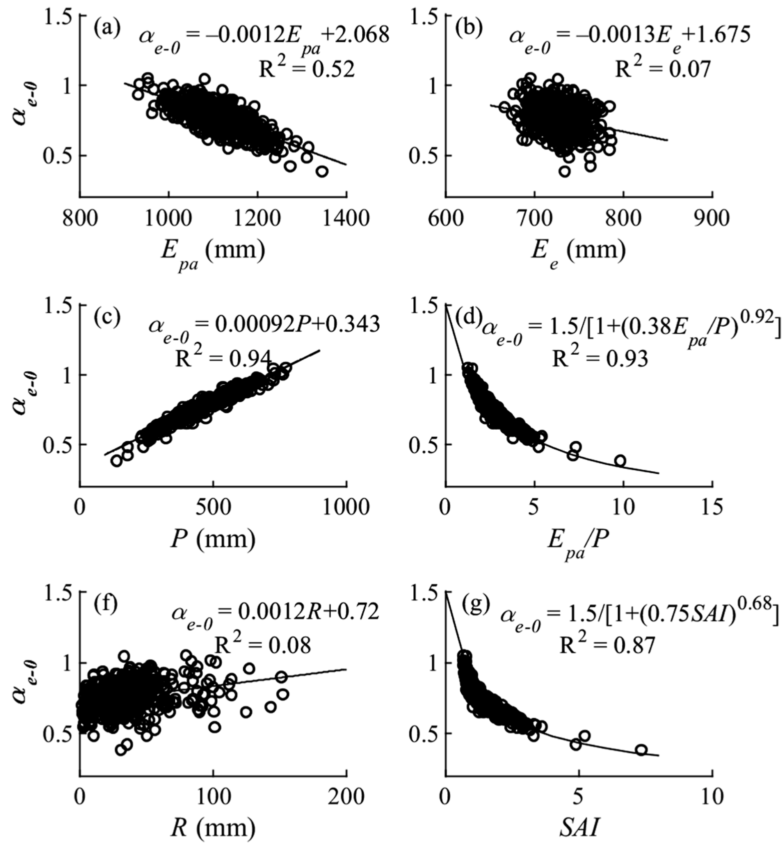

Fig. 2. Relationships between the annual $\alpha_{e\text{-}0}$ and its controlling factors for 10 catchments. Panels (a) – (g) reflect the relationships between $\alpha_{e\text{-}0}$ and apparent potential evaporation (E_{pa}), equilibrium evaporation (E_e), precipitation (P), aridity index (E_{pa}/P), runoff (R) and climate seasonality and asynchrony index (SAI), respectively.

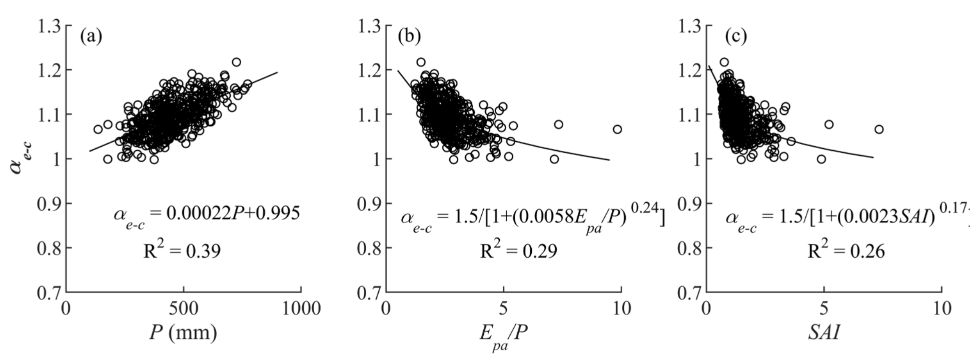

Fig. 3. Relationships between $\alpha_{e\text{-}c}$ and the controlling factors for 10 catchments. Panels (a), (b) and (c) show the relationships between $\alpha_{e\text{-}c}$ and P, E_{pa}/P, and SAI, respectively.

E_{GLEAM}, E_{0f} performed the best, with the highest R^2 in most catchments. E_{GLEAM} versus E_{0f} had the lowest MAE and RMSE in all catchments, with mean values of 50.6 and 60 mm/year, respectively (Table 2). In addition, E_{0f} could accurately approximate the amplitude in all catchments (Fig. 4). E_0 performed the worst with little fluctuation, suggesting it was incapable of capturing the interannual variation. Furthermore, E_{cf} performed better than E_c. Fig. 5 shows the relations of E_{GLEAM} with E_{0f} and E_{cf}. The data points of E_{GLEAM}–E_{0f} (magenta scatter points) distributed more closely along the 1:1 line than those of E_{GLEAM}–E_{cf}. Both E_{0f} and E_{cf} were 1.1 times E_{GLEAM}, which is consistent with the difference between E_{wb} and E_{GLEAM} (Fig. S1). The NSE value between E_{GLEAM} and E_{0f} was 0.45, larger than that between E_{GLEAM} and E_{cf}. As such, the basic GNAA form with the semi-empirical parameter function for $\alpha_{e\text{-}0}$ performed the best in estimating annual E, and could be written as follows:

$$\frac{E}{E_{pa}} = \left(2 - \frac{E_e}{E_{pa}} * \frac{1.5}{\left[1 + \left(0.38E_{pa}/P\right)^{0.92}\right]}\right) * \left(\frac{E_e}{E_{pa}} * \frac{1.5}{\left[1 + \left(0.38E_{pa}/P\right)^{0.92}\right]}\right)^2 \tag{11}$$

4. Discussion

4.1. Implications of $\alpha_{e\text{-}0}$ and $\alpha_{e\text{-}c}$

The basic GNAA form with a function of $\alpha_{e\text{-}0}$ can accurately simulate the interannual variation and estimate the annual values of E. However, most values of $\alpha_{e\text{-}0}$ were lower than 1.0 at an annual scale on the Loess Plateau. When the corrected precipitation was used, the annual average

Table 2
Comparisons of E from different parameterization methods with E_{GLEAM}.

ID	E_{GLEAM}	E_0			E_c			E_{0f}			E_{cf}		
		MAE	RMSE	R^2	MAE	RMSE	R^2	MAE	RMSE	R^2	MAE	RMSE	R^2
C1	435.2	64.3	78.7	0.01	72.4	81.8	0.21	61.7	71.2	0.57	92.9	101.2	0.44
C2	429.6	41.8	52.5	0.13	44.3	52.5	0.13	28.6	35.8	0.71	41.1	50.9	0.41
C3	285.8	65.0	76.7	0	65.4	76.1	0.07	63.3	71.6	0.63	69.7	81.1	0.40
C4	407.4	60.3	73.3	0.05	72.2	78.1	0.57	77.0	86.6	0.61	126.4	130.6	0.66
C5	276.9	48.4	59.5	0.03	63.7	72.6	0.25	57.2	67.3	0.61	41.6	51.0	0.49
C6	279.2	69.6	77.3	0.11	66.5	71.5	0.47	36.4	47.3	0.77	58.8	66.9	0.70
C7	427.6	54.3	65.9	0	85.0	107.0	0.16	39.3	49.0	0.63	59.4	77.0	0.36
C8	293.6	61.0	69.7	0.08	59.3	65.1	0.57	47.6	56.4	0.71	28.8	35.2	0.73
C9	450.5	48.0	62.9	0.02	56.0	72.2	0.08	34.9	44.6	0.60	46.5	58.5	0.31
C10	389.0	63.2	79.3	0.02	44.4	59.0	0.21	60.4	70.5	0.61	89.5	99.4	0.43
Mean	367.5	57.6	69.6	0.05	62.9	73.6	0.27	50.6	60.0	0.65	65.5	75.2	0.49

Note: The units of the Global Land Evaporation Amsterdam Model evaporation product (E_{GLEAM}), mean absolute error (MAE), and root mean square error (RMSE) are mm/year.

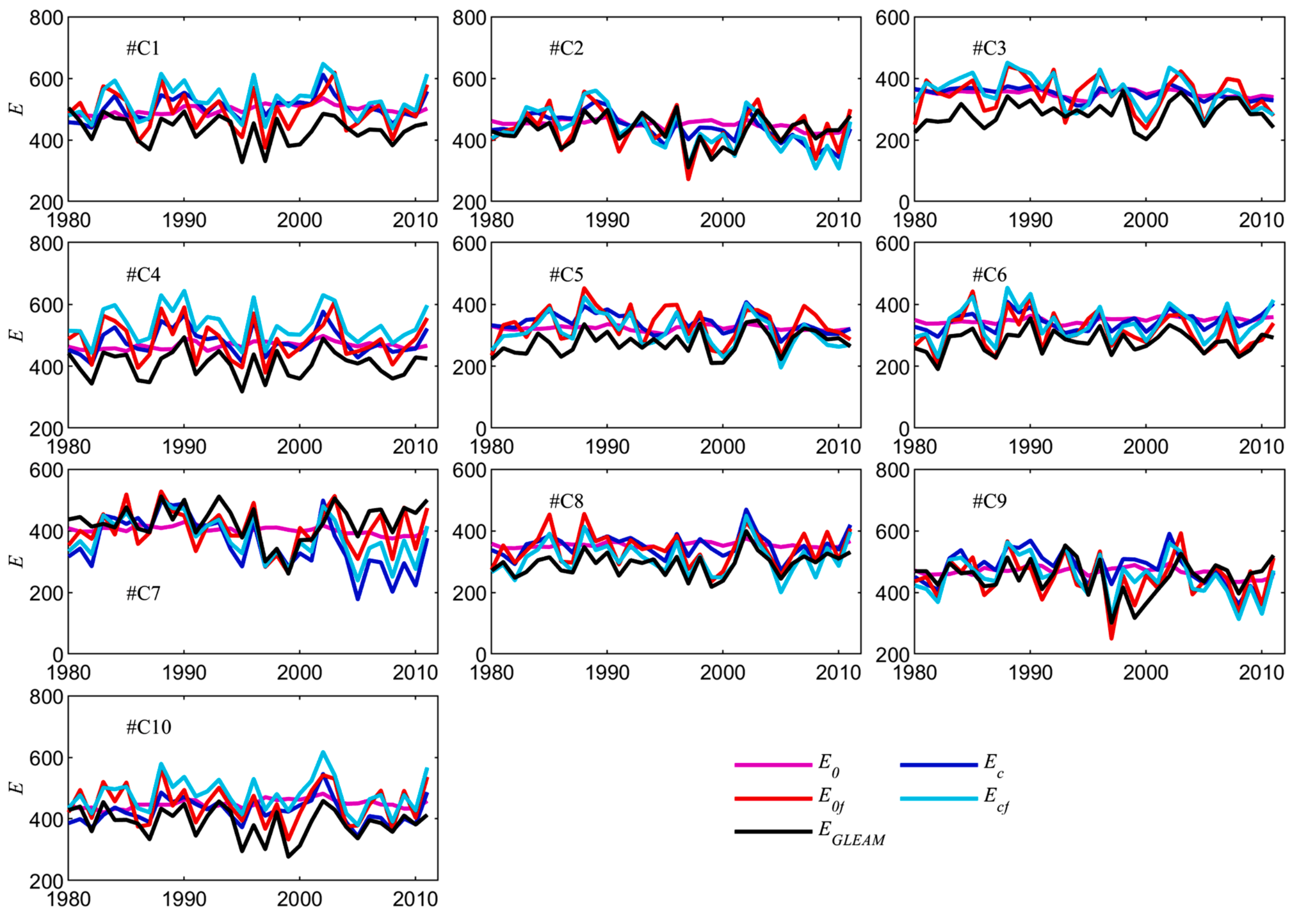

Fig. 4. Interannual variation in the evaporation rate (mm/year). E_{GLEAM} is the GLEAM evaporation dataset; E_0 and E_c are the modelled evaporation values using GNAA model with $\alpha_{e\text{-}0}$ and $\alpha_{e\text{-}c}$ (c = 6.76) for each catchment listed in Table 1; E_{0f} and E_{cf} are the modelled evaporation based on the GNAA model with the parameterization function for $\alpha_{e\text{-}0}$ and $\alpha_{e\text{-}c}$ using Eq. (9) and Eq. (10), respectively.

$\alpha_{e\text{-}0}$ were still smaller than 1.0 in each catchment. Different from the basic GNAA form, parameter $\alpha_{e\text{-}c}$ in the extended form with a fixed c value of 6.76 was larger than 1.0. The precipitation (Li et al., 2014; Liu et al., 2004) and wetness index, i.e., the reciprocal of aridity index (Gao et al., 2017; Liu et al., 2004) showed increasing trend from northwest to southeast, and $\alpha_{e\text{-}0}$ calculated by Eq. (9) had the same spatial variation as the P and wetness index (Fig. 6). More importantly, the multi-year average of $\alpha_{e\text{-}0}$ was smaller than 0.6 in the northwest and greater than 0.8 in the southeast, but was smaller than 1.0 for the whole Loess Plateau.

The boundary condition of $E = E_{po} = E_{pa}$ for a completely wet environment is the important foundation of CR. As E_{po} cannot be directly measured, it is estimated with the P-T equation in GNAA. However, it is uncertain if E_{po} can be fully quantified by the P-T equation. In the P-T equation, α accounts for the effect of advection on E enhancement (Brutsaert, 1982; de Bruin and Keijman, 1983; Lhomme, 1997). Brutsaert et al. (2017) and X. Liu et al. (2016) stated that both $\alpha_{e\text{-}0}$ and $\alpha_{e\text{-}c}$ in GNAA were only weak analogs for α in the original P-T equation, which

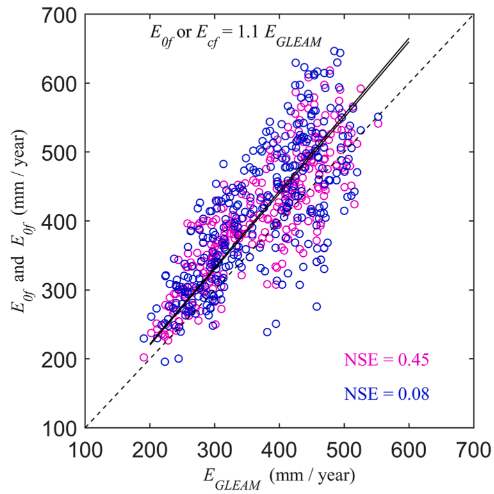

Fig. 5. Annual evaporation modelled by the GNAA model (E_{mol}) versus E_{GLEAM}. The magenta and blue points represent the E_{GLEAM}–E_{0f} and E_{GLEAM}–E_{cf} relationships, respectively.

could be adjusted to satisfy the boundary condition (Brutsaert et al., 2020). Our results show that $\alpha_{e\text{-}0}$ and $\alpha_{e\text{-}c}$ were significantly related to E_{pa}/P, P, and SAI. This indicates that $\alpha_{e\text{-}0}$ and/or $\alpha_{e\text{-}c}$ may be a compound parameters, involving the α parameter in the P-T equation and other factors.

4.2. Role of parameter c in the extended GNAA form

The determination coefficients for the relationships between $\alpha_{e\text{-}c}$ and E_{pa}/P, P, and SAI were smaller than those in the basic form, which might be due to the introduction of the c parameter. The parameter c decreased the influence of other factors on $\alpha_{e\text{-}c}$, and rendered $\alpha_{e\text{-}c}$ with a narrow variation range (from 1.00 to 1.22 for annual values), closer to the α defined by Priestley and Taylor (1972).

According to the boundary condition of y=0 as x_B =0, the GNAA theoretical curves should start from the origin and increase monotonically in the domain of [0, 1]. However, the extended GNAA form has one more intersection with the x-axis when c>2, and the intersection gradually moves to the right with increasing c. If we let the curves start from the intersection point in the interval of (0,1), it actually represents y=0 as x_B=$x_{B,min}$. Liu et al. (2020) showed that $x_{B,min}$ =[2c-1-(1+4c)$^{0.5}$]/2c. Zhou et al. (2020) found that the extended GNAA curve could capture the trend in scatterplots of E/E_{pa} versus E_{po}/E_{pa} when using a multi-year mean $\alpha_{e\text{-}c}$ parameter at a catchment scale. However, Szilagyi et al. (2020) recognized that the parameter $\alpha_{e\text{-}0}$ function of Eq. (9) rescaled x_B, which made the GNAA curve start from the origin. The parameter $\alpha_{e\text{-}c}$ in the extended GNAA was closer to the α in the P-T equation and met the lower limit requirement of the α, and the basic GNAA form of Eq. (11) performed better in E simulation than the extended form, which indicated the functional differences between the two forms of GNAA.

Previous studies tried to adopt a relatively stable $\alpha_{e\text{-}c}$, and then calibrated the parameter c in the extended GNAA (Wang et al., 2021; Zhou et al., 2020). When $\alpha_{e\text{-}c}$ was set as the mean value of 1.08 for 10 catchments, the calibrated parameter c was in the interval of [0.77, 10.48], which is larger than the range of parameter $\alpha_{e\text{-}c}$ in Table 1. As shown in Fig. S2, the relationships between parameter c and P, E_{pa}/P and SAI were opposite to those between $\alpha_{e\text{-}c}$ and these factors; that is, parameter c decreased with increasing of P, but increased with increasing E_{pa}/P and SAI. Most importantly, the fitness degree (i.e., R^2) of parameter c with the above factors was similar with that of $\alpha_{e\text{-}c}$, and thus $\alpha_{e\text{-}c}$ and c were equivalent in describing the influence of P, E_{pa}/P, and SAI when the extended GNAA form was applied. In addition, the performances of E estimation with c being calibrated or calculated with the function between c and E_{pa}/P were also evaluated with $\alpha_{e\text{-}c}$=1.08, denoted as E_{α} and $E_{\alpha f}$, respectively (Table S3). Zhou et al. (2020) found that the performance of E estimation slightly decreased when $\alpha_{e\text{-}c}$ was set as a constant value compared with the parameters of $\alpha_{e\text{-}c}$ and c being calibrated. The performance of E_{α} (i.e., the simulated E with c being calibrated and $\alpha_{e\text{-}c}$=1.08), was better than that of E_c when compared with E_{GLEAM}, but the E_{0f} was better than $E_{\alpha f}$. In conclusion, E_{0f} had the highest accuracy since the $\alpha_{e\text{-}0}$ compared with $\alpha_{e\text{-}c}$ and c, had a better fitness with E_{pa}/P.

5. Conclusions

The GNAA model is a realistic descriptor of regional evaporation, which uses only standard meteorological data. With the data from 10 catchments on the Loess Plateau, this study found that the parameters $\alpha_{e\text{-}0}$ and $\alpha_{e\text{-}c}$ in GNAA are correlated with the E_{pa}/P, P, and SAI. In particular, there is a strong relationship between $\alpha_{e\text{-}0}$ and E_{pa}/P with a determination coefficient of 0.94. The GNAA model with a function of $\alpha_{e\text{-}0}$ related to E_{pa}/P can accurately simulate E and its interannual variation on the catchment scale. It was proved that $\alpha_{e\text{-}0}$ and $\alpha_{e\text{-}c}$ are integrated parameters involving α in the P-T equation and other factors. For the extended GNAA form, when c is fixed as mean value of 6.76, the

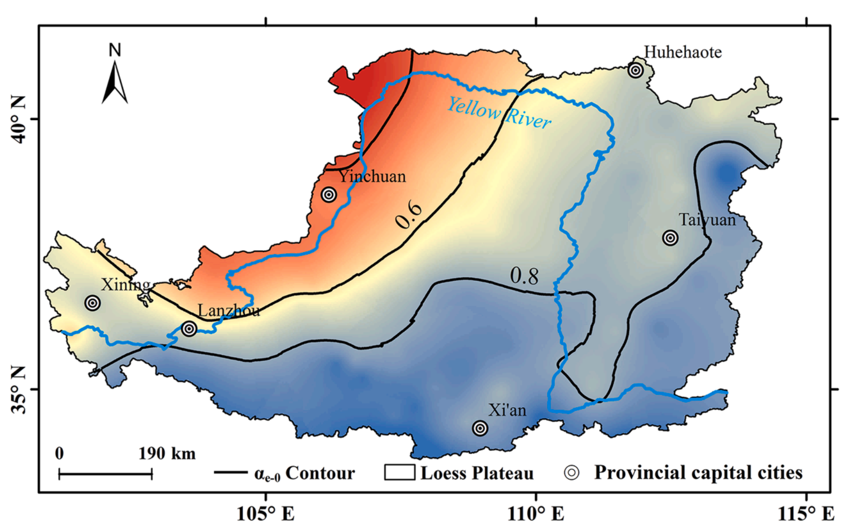

Fig. 6. Spatial distribution for parameter $\alpha_{e\text{-}0}$ on the Loess Plateau.

mean annual α_{e-c} has a narrow variation range, and is close to the parameter α in the P-T equation. With new interpretation of the parameters and understanding of functional differences between the basic and extended GNAA forms, it is found that the combination of the two forms of GNAA can better estimate evaporation and describe the relationship between E, E_{pa}, and E_{po}. The basic GNAA form is reliable and can be applied to estimate evaporation in regions with different climate types or sparse data.

Declaration of Competing Interest

None.

Acknowledgments

This study was supported by the National Natural Science Foundation of China [grant number 41971049] and the National Key Research and Development Program of China [grant number 2016YFC0501602]. Daily climate data were collected from 123 weather station maintained by the China Meteorological Administration (http://data.cma.cn/) for the period from 1960 to 2012. Runoff data were collected from the Loess Plateau Data Center (http://loess.geodata.cn). The authors wish to thank the anonymous reviewers for their valuable suggestions that greatly improved the original manuscript.

Supplementary materials

Supplementary material associated with this article can be found, in the online version, at doi:10.1016/j.agrformet.2021.108343.

References

Ai, Z., Wang, Q., Yang, Y., Manevski, K., Zhao, X., Eer, D., 2017. Estimation of land–surface evaporation at four forest sites across Japan with the new nonlinear complementary method. Sci. Rep. 7 (1), 17793. https://doi.org/10.1038/s41598-017-17473-0.

Allen, R.G., Pereira, L.S., Raes, D., Smith, M., 1998. Crop Evapotranspiration—Guidelines for Computing Crop Water Requirements. Food and Agri. Organization, Rome, Italy.

Berghuijs, W.R., Woods, R.A., 2016. A simple framework to quantitatively describe monthly precipitation and temperature climatology. Int. J. Climatol. 36 (9), 3161–3174. https://doi.org/10.1002/joc.4544.

Bouchet, R.J., 1963. Evapotranspiration réelle et potentielle, signification climatique. Int. Assoc. Hydrolog. Sci. Publ. 62, 134–142.

Brutsaert, W., 1982. Evaporation into the Atmosphere: Theory, History, and Applications. Kluwer Academic, Dordrecht.

Brutsaert, W., 2015. A generalized complementary principle with physical constraints for land–surface evaporation. Water Resour. Res. 51 (10), 8087–8093. https://doi.org/10.1002/2015WR017720.

Brutsaert, W., Cheng, L., Zhang, L., 2020. Spatial distribution of global landscape evaporation in the early twenty first century by means of a generalized complementary approach. J. Hydrometeorol. 21 (02), 287–298. https://doi.org/10.1175/JHM-D-19-0208.1.

Brutsaert, W., Li, W., Takahashi, A., Hiyama, T., Zhang, L., Liu, W., 2017. Nonlinear advection-aridity method for landscape evaporation and its application during the growing season in the southern Loess Plateau of the Yellow River basin. Water Resour. Res. 53 (1), 270–282. https://doi.org/10.1002/2016WR019472.

Brutsaert, W., Stricker, H., 1979. An advection-aridity approach to estimate actual regional evapotranspiration. Water Resour. Res. 15 (2), 443–450. https://doi.org/10.1029/WR015i002p00443.

Budyko, M.I., 1948. Evaporation under natural conditions, Gidrometeorizdat, Leningrad. English translation by IPST, Jerusalem.

Budyko, M.I., 1974. Climate and Life. Academic, New York.

Carmona, A.M., Sivapalan, M., Yaeger, M.A., Poveda, G., 2014. Regional patterns of interannual variability of catchment water balances across the continental US: A Budyko framework. Water Resour. Res. 50 (12), 9177–9193. https://doi.org/10.1002/2014WR016013.

Chen, D., Brutsaert, W., 1995. Diagnostics of land surface spatial variability and water vapor flux. J. Geophys. Res. 100, 25595–25606. https://doi.org/10.1029/95JD00973.

Chen, F., Dudhia, J.J.M.W.R., 2001. Coupling an advanced land surface-hydrology model with the Penn State-NCAR MM5 modeling system. Part I: model implementation and sensitivity. Month. Weather Rev. 129 (4), 569–585. https://doi.org/10.1175/1520-0493(2001)129<0569:CAALSH>2.0.CO;2.

de Bruin, H.A.R., Keijman, J.Q., 1983. A model for the Priestley–Taylor parameter α. J. Clim. Appl. Meteorol. 22 (4), 572–580. https://doi.org/10.1175/1520-0450(1983)022<0572:AMFTPT>2.0.CO;2.

Delhomme, J.P., 1987. Kriging in the hydrosciences. Adv. Water Resour. (5), 251–266. https://doi.org/10.1016/0309-1708(78)90039-8.

Feng, X., Fu, B., Piao, S., Wang, S., Ciais, P., Zeng, Z., Lü, Y., Zeng, Y., Li, Y., Jiang, X., 2016. Revegetation in China's Loess Plateau is approaching sustainable water resource limits. Nat. Clim. Change 6 (11). https://doi.org/10.1038/NCLIMATE3092, 1019-+.

Fu, B., Chen, L., Ma, K., Zhou, H., Wang, J., 2000. The relationships between land use and soil conditions in the hilly area of the loess plateau in northern Shaanxi, China. Catena 39 (1), 69–78. https://doi.org/10.1016/S0341-8162(99)00084-3.

Gao, B., Xu, X., 2020. Derivation of an exponential complementary function with physical constraints for land surface evaporation estimation. J. Hydrol. https://doi.org/10.1016/j.jhydrol.2020.125623.

Gao, X., Zhao, Q., Zhao, X., Wu, P., Pan, W., Gao, X., Sun, M., 2017. Temporal and spatial evolution of the standardized precipitation evapotranspiration index (SPEI) in the Loess Plateau under climate change from 2001 to 2050. Sci. Total Environ. 595, 191–200. https://doi.org/10.1016/j.scitotenv.2017.03.226.

Goodison, B.E., Sevruk, B., Klemm, S., 1989. WMO Solid Precipitation Measurement Intercomparison: Objectives, Methodology, Analysis. Int. Assoc. Hydrolog. Sci. Publ. 179, 57–64.

Granger, R.J., 1989. A complementary relationship approach for evaporation from nonsaturated surfaces. J. Hydrol. 111 (1–4), 0–38. https://doi.org/10.1016/0022-1694(89)90250-3.

Han, S., Tian, F., 2018. Derivation of a sigmoid generalized complementary function for evaporation with physical constraints. Water Resour. Res. 54 (7), 5050–5068. https://doi.org/10.1029/2017WR021755.

Han, S., Tian, F., 2020. A review of the complementary principle of evaporation: from the original linear relationship to generalized nonlinear functions. Hydrol. Earth Syst. Sc. 24 (5), 2269–2285. https://doi.org/10.5194/hess-24-2269-2020.

Han, S., Hu, H., Tian, F., 2012. A nonlinear function approach for the normalized complementary relationship evaporation model. Hydrol. Processes 26 (26), 3973–3981. https://doi.org/10.1002/hyp.8414.

Hu, Z., Wang, G., Sun, X., Zhu, M., Song, C., Huang, K., Chen, X., 2018. Spatial–temporal patterns of evapotranspiration along an elevation gradient on mount gongga, southwest China. Water Resour. Res. 54 (6), 4180–4192. https://doi.org/10.1029/2018WR022645.

Jimenez, C., Prigent, C., Mueller, B., Seneviratne, S.I., McCabe, M.F., Wood, E.F., Rossow, W.B., Balsamo, G., Betts, A.K., Dirmeyer, P.A., Fisher, J.B., Jung, M., Kanamitsu, M., Reichle, R.H., Reichstein, M., Rodell, M., Sheffield, J., Tu, K., Wang, K., 2011. Global intercomparison of 12 land surface heat flux estimates. J. Geophys. Res. 116, D02102. https://doi.org/10.1029/2010JD014545.

Jung, M., Reichstein, M., Margolis, H.A., Cescatti, A., Richardson, A.D., Arain, M.A., Arneth, A., Bernhofer, C., Bonal, D., Chen, J.Q., Gianelle, D., Gobron, N., Kiely, G., Kutsch, W., Lasslop, G., Law, B.E., Lindroth, A., Merbold, L., Montagnani, L., Moors, E.J., Papale, D., Sottocornola, M., Vaccari, F., Williams, C., 2011. Global patterns of land-atmosphere fluxes of carbon dioxide, latent heat, and sensible heat derived from eddy covariance, satellite, and meteorological observations. J. Geophys. Res. 116, G00J07. https://doi.org/10.1029/2010JG001566.

Lhomme, J.P., 1997. A theoretical basis for the Priestley–Taylor coefficient. Bound.–Lay. Meteorol. 82 (2), 179–191. https://doi.org/10.1023/A:1000281114105.

Li, T., Xia, J., Zhang, L., She, D., Wang, G., Cheng, L., 2021. An improved complementary relationship for estimating evapotranspiration attributed to climate change and revegetation in the Loess Plateau, China. J. Hydrol. 592. https://doi.org/10.1016/j.jhydrol.2020.125516.

Li, Z., Brissette, F., Chen, J., 2014. Assessing the applicability of six precipitation probability distribution models on the Loess Plateau of China. Int. J. Climatol. 34 (2), 462–471. https://doi.org/10.1002/joc.3699.

Liu, C., Zeng, Y., Qiu, X., 2004. Altas of Meteo–Hydrologyic Elements in the Yellow River basin. The Yellow River Water Conservancy Press (in Chinese).

Liu, J., Zhang, Q., Singh, V.P., Song, C., Zhang, Y., Sun, P., Gu, X., 2018. Hydrological effects of climate variability and vegetation dynamics on annual fluvial water balance in global large river basins. Hydrol. Earth Syst. Sc. 22 (7), 4047–4060. https://doi.org/10.5194/hess-22-4047-2018.

Liu, W., Wang, L., Zhou, J., Li, Y., Sun, F., Fu, G., Li, X., Sang, Y.-F., 2016. A worldwide evaluation of basin–scale evapotranspiration estimates against the water balance method. J. Hydrol. 538, 82–95. https://doi.org/10.1016/j.jhydrol.2016.04.006.

Liu, W., Zhou, H., Han, X., Li, Z., 2020. Comment on two papers about the generalized complementary evaporation relationships by Crago et al. Water Resour. Res. 56 (3), e2019WR026292 https://doi.org/10.1029/2019WR026292.

Liu, X., Liu, C., Brutsaert, W., 2016. Regional evaporation estimates in the eastern monsoon region of China: assessment of a nonlinear formulation of the complementary principle. Water Resour. Res. 52 (12), 9511–9521. https://doi.org/10.1002/2016WR019340.

Liu, X., Liu, C., Brutsaert, W., 2018. Investigation of a generalized nonlinear form of the complementary principle for evaporation estimation. J.Geophys. Res.– Atmos. 123 (8), 3933–3942. https://doi.org/10.1002/2017jd028035.

Lv, M., Ma, Z., Li, M., Zheng, Z., 2019. Quantitative analysis of terrestrial water storage changes under the grain for green program in the Yellow River Basin. J. Geophys. Res.–Atmos. 124 (3), 1336–1351. https://doi.org/10.1029/2018JD029113.

Ma, N., Szilagyi, J., Zhang, Y., Liu, W., 2019. Complementary-relationship-based modeling of terrestrial evapotranspiration across China during 1982–2012: validations and spatiotemporal analyses. J. Geophys. Res.–Atmos. 124 (8), 4326–4351. https://doi.org/10.1029/2018JD029850.

Martens, B., Miralles, D.G., Lievens, H., van der Schalie, R., de Jeu, R.A.M., Fernandez-Prieto, D., Beck, H.E., Dorigo, W.A., Verhoest, N.E.C., 2017. GLEAM v3: Satellite-based land evaporation and root-zone soil moisture. Geosci. Model Dev. 10 (5), 1903–1925. https://doi.org/10.5194/gmd-10-1903-2017.

Milly, P.C.D., 1994. Climate, soil–water storage, and the average annual water–*b*alance. Water Resour. Res. 30 (7), 2143–2156. https://doi.org/10.1029/94WR00586.

Mo, X., Wu, J.J., Wang, Q., Zhou, H., 2016. Variations in water storage in China over recent decades from GRACE observations and GLDAS. Nat. Hazard. Earth Sys. 16 (2), 469–482. https://doi.org/10.5194/nhess-16-469-2016.

Morton, F.I., 1978. Estimating evapotranspiration from potential evaporation: practicality of an iconoclastic approach. J. Hydrol. 38 (1–2), 0–32. https://doi.org/10.1016/0022-1694(78)90129-4.

Morton, F.I., 1983. Operational estimates of areal evapotranspiration and their significance to the science and practice of hydrology. J. Hydrol. 66 (1), 1–76. https://doi.org/10.1016/0022-1694(83)90177-4.

Ning, T., Zhou, S., Chang, F., Shen, H., Li, Z., Liu, W., 2019. Interaction of vegetation, climate and topography on evapotranspiration modelling at different time scales within the Budyko framework. Agr. Forest Meteorol. 275, 59–68. https://doi.org/10.1016/j.agrformet.2019.05.001.

Ning, T., Feng, Q., LI, Z., Li, Z., 2020. Recent changes in climate seasonality in the inland river basin of Northwestern China. J. Hydrol. 590, 125212 https://doi.org/10.1016/j.jhydrol.2020.125212.

Penman, H.L., 1948. Natural evaporation from open water, bare soil and grass. Proceed. R. Soc. Lond. A: Math. Phys. Eng. Sci. 193, 120–146. https://doi.org/10.1098/rspa.1948.0037.

Priestley, C.H.B., Taylor, R.J., 1972. On the assessment of sur face heat flux and evaporation using large–scale parameters. Month. Weather Rev. 100 (2), 81–92. https://doi.org/10.1175/1520-04931972)100<0081:otaosh>2.3.co;2.

Sevruk, B., Hamon, W.R., 1984. International comparison of national precipitation gauges with a reference pit gauge. In: WMO Instrum. Observ. Methods Rep., 17. WMO, p. 111.

Sivapalan, M., Yaeger, M.A., Harman, C.J., Xu, X., Troch, P.A., 2011. Functional model of water balance variability at the catchment scale: 1. evidence of hydrologic similarity and space-time symmetry. Water Resour. Res. 47 (2), 2144–2150. https://doi.org/10.1029/2010wr009568.

Slatyer, R.O., Mcilroy, I.C., 1961. Pract. Microclimatol. CSIRO. 310.

Szilagyi, J., Crago, R., Ma, N., 2020. Dynamic scaling of the generalized complementary relationship improves long-term tendency estimates in land evaporation. Adv. Atmos. Sci. 37 (9), 975–986. https://doi.org/10.1007/s00376-020-0079-6.

Szilagyi, J., Crago, R., Qualls, R., 2016. Testing the generalized complementary relationship of evaporation with continental–scale long–term water–*b*alance data. J. Hydrol. 540, 914–922. https://doi.org/10.1016/j.jhydrol.2016.07.001.

Tang, K., 1998. Discussion on key problem of eco–environment construction on Loess Plateau. Bull. Soil Water Conserv. 18 (1), 12–14. https://doi.org/10.14123/j.cnki.swcc.1985.12.003 (in Chinese).

Wang, Liming, Han, Songjun, Tian, Fuqiang, 2021. At which timescale does the complementary principle perform best in evaporation estimation? Hydrol. Earth Syst. Sci. 25 (1), 375–386. https://doi.org/10.5194/hess-25-375-2021.

Woods, R., 2003. The relative roles of climate, soil, vegetation and topography in determining seasonal and long–term catchment dynamics. Adv. Water Resour. 26 (3), 295–309. https://doi.org/10.1016/S0309-1708(02)00164-1.

Xue, B., Wang, L., Li, X., Yang, K., Chen, D., Sun, L., 2013. Evaluation of evapotranspiration estimates for two river basins on the Tibetan Plateau by a water balance method. J. Hydrol. 492, 290–297. https://doi.org/10.1016/j.jhydrol.2013.04.005.

Yang, D., Goodison, B.E., Metcalfe, J.R., Louie, P., Leavesley, G., Emerson, D., Hanson, C. L., Golubev, V.S., Elomaa, E., Gunther, T., 1999. Quantification of precipitation measurement discontinuity induced by wind shields on national gauges. Water Resour. Res. 35, 491–508. https://doi.org/10.1029/1998WR900042.

Yang, H., Yang, D., Lei, Z., 2013. Seasonal variability of the complementary relationship in the Asian monsoon region. Hydrol. Processes 27 (19), 2736–2741. https://doi.org/10.1002/hyp.9400.

Yang, X., Yong, B., Yin, Y., Zhang, Y., 2018. Spatio–temporal changes in evapotranspiration over China using GLEAM_V3.0a products (1980–2014). Hydrol. Res. 49 (5), 1330–1348. https://doi.org/10.2166/nh.2018.173.

Yu, X., Yang, H., Lv, H., Huang, F., 2019. Generalized evapotranspiration–complementarity theory–*b*ased analysis on variation of actual evapotranspiration in oases of Tarim River Basin and its attribution. Water Resour. Hydropower Eng. 1–17 (in Chinese).

Zhang, B., Xia, Y., Long, B., Hobbins, M., Zhao, X., Hain, C., Li, Y., Anderson, M.C., 2020. Evaluation and comparison of multiple evapotranspiration data models over the contiguous United States: Implications for the next phase of NLDAS (NLDAS-Testbed) development. Agr. Forest Meteorol. 280 https://doi.org/10.1016/j.agrformet.2019.107810.

Zhang, L., Cheng, L., Brutsaert, W., 2017. Estimation of land surface evaporation using a generalized nonlinear complementary relationship. J. Geophys. Res.–Atmos. 122 (3), 1475–1487. https://doi.org/10.1002/2016jd025936.

Zhang, X., Zhang, L., Zhao, J., Rustomji, P., Hairsine, P., 2008. Responses of streamflow to changes in climate and land use/cover in the Loess Plateau, China. Water Resour. Res. 44 https://doi.org/10.1029/2007wr006711.

Zhang, Y., Penaarancibia, J.L., Mcvicar, T.R., Chiew, F.H.S., Vaze, J., Liu, C., Lu, X., Zheng, H., Wang, Y., Liu, Y.Y.J.S.R., 2016. Multi-decadal trends in global terrestrial evapotranspiration and its components. Sci. Rep. 6 (1), 19124. https://doi.org/10.1038/srep19124.

Zhao, Q., Liu, X., Ditmar, P., Siemes, C., Revtova, E., Hashemi-Farahani, H., Klees, R., 2011. Water storage variations of the Yangtze, Yellow, and Zhujiang river basins derived from the DEOS mass transport (DMT–1) model. Sci. China Earth Sci 54 (5), 667–677. https://doi.org/10.1007/s11430-010-4096-7.

Zhou, H., Han, S., Liu, W., 2020. Evaluation of two generalized complementary functions for annual evaporation estimation on the Loess Plateau, China. J. Hydrol. 58 https://doi.org/10.1016/j.jhydrol.2020.124980.